

MULTIMODAL OBJECT DETECTION VIA PROBABILISTIC A PRIORI INFORMATION INTEGRATION

1st Hafsa El Hafyani
IMT Atlantique
Lab-STICC, UMR CNRS 6285
Brest F-29238, France
hafsa.el-hafyani@imt-atlantique.fr

2nd Bastien Padeloup
IMT Atlantique
Lab-STICC, UMR CNRS 6285
Brest F-29238, France
bastien.padeloup@imt-atlantique.fr

3rd Camille Yver
InPixaI
Rennes, France
camille.yver@inpixal.com

4th Pierre Romenteau
InPixaI
Rennes, France
pierre.romenteau@inpixal.com

Abstract—Multimodal object detection has shown promise in remote sensing. However, multimodal data frequently encounter the problem of low-quality, wherein the modalities lack strict cell-to-cell alignment, leading to mismatch between different modalities. In this paper, we investigate multimodal object detection where only one modality contains the target object and the others provide crucial contextual information. We propose to resolve the alignment problem by converting the contextual binary information into probability maps. We then propose an early fusion architecture that we validate with extensive experiments on the DOTA dataset.

Index Terms—Object detection, Multimodal fusion, deep learning, alignment, remote sensing

I. INTRODUCTION

Object detection has made remarkable progress thanks to the advances of deep neural detectors. While this thematic is generally developed based on ground level sensors images, applying classical object detection techniques ([1] [2]) directly to aerial or space images (e.g. satellite and/or drone images) results in reduced performance. Remote sensing images present more complicated background information, larger scale variance and densely small targets. Therefore, practical applications, such as military surveillance of areal images leverage multimodal data to enhance object detection capabilities, by incorporating complementary information modelling the structure and context of the objects in the scene.

However, when complementary information is collected by multiple sensors or sources (e.g., land cover/use, SAM [3]), it may present problems of low quality or misalignment with the acquired images, due to, for instance, angular acquisition, leading to potential errors in detection. Figure 1 presents an example of low-quality problem of the contextual information (i.e. masks) acquired by three different sensors. Neither of the contextual information matches perfectly the aerial image. The masks of roundabouts (i.e. left) and vehicles (i.e. right)

collected by two different sensors show a shift w.r.t. the aerial image (i.e. center). Therefore, it is crucial to present the combination of different modalities in a cohesive manner. Failure to align one modality with the others could lead to increased errors in detection.

While showing considerable promise in multimodal tasks ([4], [5]), the performance of object detectors in mis-aligned multimodal geospatial settings is to be verified. Therefore, this paper first investigates the performance of multimodal data compared to unimodal data for geospatial tasks, since multimodal data do not necessarily improve performance [6]. Second, we suggest to resolve the mis-alignment issue by transforming contextual information into probability maps. Third, we examine the proposed alignment approach performance compared to no-alignment settings using the DOTA dataset [7].

The rest of this paper is organized as follows. We introduce the related work in Section II. Section III gives a thorough problem description, describes the proposed approach for resolving the alignment issue, and discuss the proposed fusion models. Section IV presents the experimental results and evaluation of the multimodal fusion detectors. Last but not least, in section V, we summarize our conclusions and provide directions for future work.

II. RELATED WORK

A. Generic Object Detection Methods

Deep learning-based algorithms are widely used for object detection with two main categories: two-stage and single-stage approaches. Two-stage methods, such as Faster-RCNN [8], have better detection accuracy as they initially generate candidate boxes, and then identify the object category and refine the object location. One-stage methods, such as SSD [1] and YOLO series [2], offer faster inference speeds since the



Fig. 1: Example of misalignment of contextual data with an acquired RGB image. On the left, the mask of roundabout does not match the RGB image (center). On the right, the mask of vehicles shows a shift w.r.t. the RGB image.

proposals generation is not needed. Although these methods have shown a good performance on images taken from the ground level, the same performance is not achieved on remote sensing images due to the complex nature of aerial images.

On top of that, modern detectors adopt an encoder-decoder architecture based on transformers [9]–[11]. Specifically, Carion *et al.* [12] and Zhu *et al.* propose new models called DETR and Deformable DETR, respectively, which have shown competitive results to Faster-RCNN model on large objects. DETR performs less effectively for small objects [12]. Additionally, Kirillov *et al.* unveiled SAM [3], a highly accurate pre-trained model for diverse image types, including remote sensing images. Researchers are exploring its potential in handling multimodal data scenarios.

B. Deep Multimodal Fusion

Researchers have explored various approaches for implementing multimodal fusion to enhance the performance of object detectors in remote sensing. Zhang *et al.* [4] propose a contextual bidirectional enhancement method to enhance objects’ features. Chen *et al.* [5] propose to combine scene-contextual information in a convolutional neural network to improve the relationship between scene and target. Besides aerial images, several works on the multimodal fusion exist in the literature. Gao *et al.* [13] review different approaches to represent multimodal data, and Chu *et al.* [14] present MT-DETR, a new fusion model through early and late fusion. Even though these methods have shown good performances when combined with contextual information or other modalities, the alignment problem was not addressed.

C. Image Alignment

Image alignment is not a new task for the computer vision research community. Brown [15] provides a comprehensive review of methods involving geometric transformations to align images based on criteria like similarity. Building upon these approaches, Wang *et al.* [16] successfully aligned and merged RGB images with thermal images. Girard *et al.* [17] proposed a fully convolutional architecture to correct the alignment of building registries (*e.g.*, from OpenStreetMap) on the image. To handle the weakly aligned multispectral data, which makes one object has different positions in different modalities, Zhang *et al.* [18] proposed a novel Aligned Region CNN (AR-CNN), which includes a region feature alignment module to align the region features. following the work of

Zhang *et al.* [18], Yuan *et al.* [19] propose an end-to-end model called CAGT to solve weak misalignment and fusion imprecision problem in regional level in multispectral data. Therefore, image alignment has proven successful in these studies, particularly when dealing with two images that depict the same aspects (*e.g.*, RGB images and thermal images) and both exhibit the target objects. However, when attempting to align RGB images with binary masks, the task becomes more and more challenging.

III. CONTRIBUTIONS

A. Problem Statement

We consider a problem that involves two domains, a *multimodal object detection problem* [13] of RGB images and contextual information represented by binary masks retrieved by sensors or segmentation models (*e.g.* SAM), showing the land cover/use data, and *image alignment problem* ([17], [20], [21]) between different modalities.

Existing work on modality alignment mainly emphasizes datasets where objects are visible across all modalities. However, in our case, objects are exclusively visible within one modality. The alignment of these unique characteristic modalities requires the development of specialized techniques tailored to address this specific circumstance. Traditional approaches may not be directly applicable here, since they are based on the assumption of object presence across multiple modalities. Therefore, innovative solutions are necessitated to effectively align modalities and fill the gap of modality alignment in the case of the absence of object visibility across all modalities in the dataset.

Our objective is to train a detector that can combine the multimodal data while ensuring a sound cross-modality representation. Specifically, we desire to obtain an agnostic shift alignment representation that works equally whether the multi modalities are shifted or not. Therefore, we propose a multimodal fusion model for object detection based on probability maps. Indeed, instead of having binary values (*i.e.*, 0 and 1), the probability map assigns a continuous value between 0 and 1 to each pixel, indicating the probability of that pixel hosting the object. Hence, even if the modalities are not perfectly aligned, the probability maps can provide guidance to the model and inform it about the likelihood of the object’s presence within the cell.

B. Probability Maps

One straightforward way to generate probabilistic maps is the Euclidean distance transformation. Inspired by common sense, it consists of calculating the Euclidean distance of each pixel to the nearest boundary (pixel with a value of 1) in the binary image. As the distance between a pixel and the object’s boundary increases, its probability of hosting the object decreases. Formally, the task involves processing a single channel image represented as a tensor I_c of size $H * W * 1$, where each element $I_c(i, j)$ is either 0 or 1. H and W denote image’s height and the width, respectively. We want to compute the probability map P of the same size, where

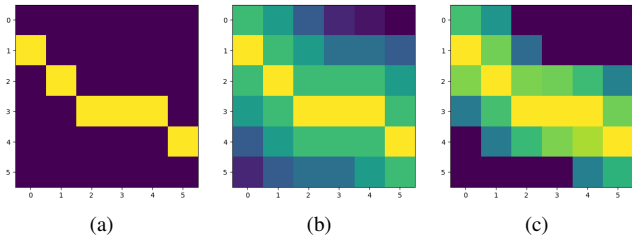


Fig. 2: Example of the construction of probability maps from a binary mask (a) based on Eq. 1 (b) and Eq. 2 (c).

each element $P(i, j)$ represents the probability of the pixel at position (i, j) belonging to the target class:

$$\begin{cases} P(i, j) = 1 - d_{norm}(i, j) \\ d_{norm}(i, j) = \frac{d(i, j)}{\max(d)} \\ d(i, j) = \min_{i', j' s.t. (i', j') \in I_c} \|(i, j) - (i', j')\|_2 \end{cases} \quad (1)$$

where $d_{norm}(i, j)$ is normalized distance from each cell to the object, and $d(i, j)$ is the Euclidean distance of pixel at position (i, j) to the nearest boundary.

Figure 2 shows an example of the generation of these maps (Figure 2b) from a binary mask (Figure 2a). The probability is higher for pixels closer to the object boundary and decreases as the distance from the object boundary increases. As a matter of fact, the above representation of probability maps based on the Euclidean distance shows a smooth propagation of the mask through the whole image. However, the pixel with the coordinates $(1, 1)$ in Figure 2b should have a higher probability since it is a neighbour of two cells hosting the object (*i.e.*, cells with coordinates $(0, 1)$ and $(1, 2)$), as it would be resilient to misalignments along two axes rather than one. Therefore, we propose an alternative distance for constructing the probability maps from the binary masks. It takes into consideration both the distance to the boundaries, and the neighbouring cells as follows:

$$\forall p \in I_c, \quad d(p) = \frac{\sum_{r \in R(p)} \exp(-\alpha d(r, p))}{\sum_{m \in M} \exp(-\alpha d(m, p))} \quad (2)$$

where $R(p)$ is the set of neighbouring cells in a specific radius (to be defined by the user), $\alpha \in \mathbf{R}$ (to be set by the user as well), and M is the set of all the cells containing the mask. Therefore, with this new representation, the example shown in Figure 2a becomes as indicated in Figure 2c with $\alpha = 1$ and the radius set to 1 cell in every direction (*i.e.*, left, right, up, down, and diagonal).

C. Proposed Method

The misalignment problem is resolved with the probability maps, we introduce thereafter the flow diagram of our framework. As presented in Figure 3, the framework provides an illustration of the fusion’s logic. First, we start by generating the probability maps from the binary masks using either equation 1 or equation 2. Then, the generated probabilities

maps are concatenated to the RGB image, which is then fed to an object detector (e.g. Faster-RCNN). Finally, The detector produces the candidate classes and their bounding boxes with a feature pyramid network (FPN) based network.

IV. EXPERIMENTS

A. Dataset

Because of the sensibility of military data, we recreate the multi modality miss-alignment problem with a subset of the DOTA dataset [7] with its 15 classes as shown in Table I. The binary masks are extracted from the iSAID dataset [22].

B. Experimental Setup

We kept the training set as established by the DOTA dataset. However, we split the validation set between the validation set and testing set, since the binary masks are only provided for the training and validation sets. Therefore, 2/3 of the DOTA validation set goes to the validation set and 1/3 goes to the test set. For the evaluation metrics, we employ the widely used average precision (AP) to evaluate the performance of our model over every class, and the mean average precision (mAP), which is computed over all classes. Additionally, a candidate bounding box is considered as a true positive if the value of Intersection-Over-Union (IoU) metric is greater than 0.5; otherwise, it is a false positive. All the experiments were made by training a Faster-RCNN [8] model, initialized with COCO pre-trained weights. We inject a random shift between 5% and 10% of the image width in the binary mask to simulate the misalignment problems. Our implementation is based on the PyTorch framework under Ubuntu 20.04. The experiments were executed on NVIDIA GeForce RTX 3090. The models were trained on 50 epochs, with a batch size of 8, SGD optimizer, weight decay of $5e-4$, momentum of 0.9, and the learning rate set to 0.001. The source code will be publicly available at: https://github.com/helhafyani/Multimodal_fusion.

C. Experimental Results

We perform two types of fusion experiments to evaluate the model’s response to the integration of contextual information. The first type involves adding direct contextual information such as the inclusion of shifted, low-quality masks of objects already present in the RGB images (e.g., adding a shifted mask of boats to enhance boat’s detection). The second type explores fusion with indirect contextual information, such as shifted masks of elements like harbors to observe their impact on the model’s ability to detect specific objects (e.g. boats).

1) *Does fusion improve detection performance?:* We perform the direct fusion model with 15-class object detection and 15 binary masks (a binary mask for every class). For the indirect fusion model, we keep the 15 classes in the detection target classes, and use 3 masks: the mask of harbors is leveraged for the detection of ships, and the masks of bridges and roundabouts are adopted to to enhance the detection of small and large vehicles. We report the results in Table I. **Basic** model refers to the model without fusion. **“Distance in Eq1”** points to the fusion with the

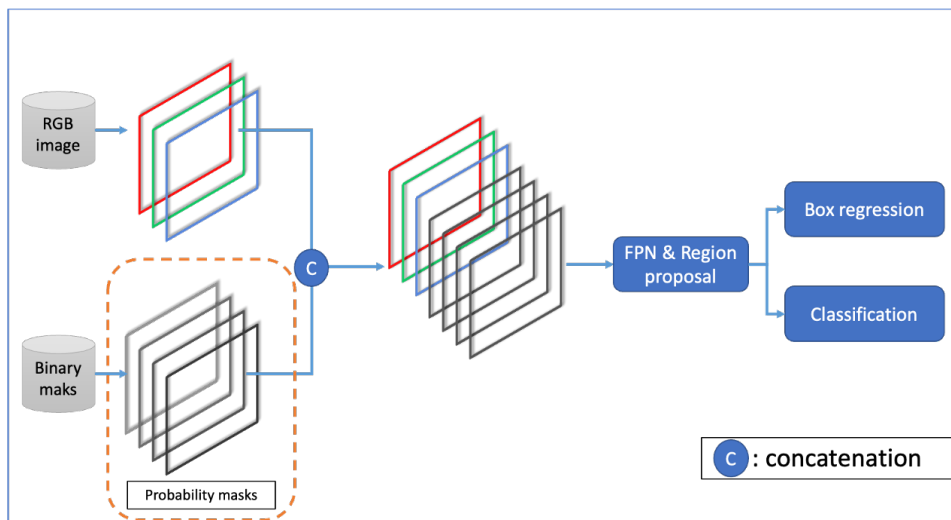


Fig. 3: The pipeline of our framework.

probability maps based on Equation 1, and “*Distance in Eq2*” relates to the fusion with probability maps based on Equation 2. **Basic fusion** model is the baseline which refers to the standard fusion model without adopting the probability maps solution.

Overall, all of the fusion models perform better than the basic model (*i.e.*, without fusion) when looking at the mAP, which indicates that adding either direct or indirect contextual information brings along a better distinction between classes. Also, although the direct fusion models show undoubtedly the highest performances, the indirect fusion models show a remarkable performance with the few added contextual information. The indirect model does not only demonstrate a better performance for the related classes, especially *ship* and *large vehicle*, but it facilitates the discrimination between the other classes. Compared to the direct fusion model (*i.e.* without the probability maps), both direct models perform better, which means adding probability maps improves the detection performance of the models. However, the indirect models have a similar performance in terms of mAP. Still, the models with probability maps perform better in detecting the classes with the contextual information, especially *ship* and *small vehicle*.

2) *Which contextual information improves class discrimination?*: To answer this question, we only add a single mask as additional input, and report the obtained performance for each class individually in Table II. The matrix diagonal can be understood as a direct fusion process with only the target class used as contextual information, while off-diagonal entries show the indirect fusion, *i.e.*, the impact of the contextual class for detecting other classes.

While it appears that adding an input layer for a probability map helps in the detection process in many cases, straightforward conclusions are not so easy. Indeed, the original reasoning behind this work was that presence of a bridge or a roundabout would probably lead to improved

detection performance for small and large vehicles. However, here, we observe marginal or no improvement at all. The same observation holds for harbor, that only brings a marginal gain for detection of ships. However, we observe that adding a layer for planes brings a 12pt gain for basketball courts, or that adding a layer for small vehicles improves detection of baseball diamonds by 10pt, which is hard to understand semantically speaking. Regarding the direct fusion though, we observe that the best performance was achieved for 4 classes out of the 15, and that performance was either improved or stayed the same for 10 of these classes. This suggests again that a priori knowledge of an element in the image improves its detection, even when we have an approximate idea of its location due to misalignments.

V. CONCLUSION & PERSPECTIVES

We explore the effectiveness of multimodal data compared to unimodal for geospatial detection. We introduce a solution to mitigate the misalignment issue, involving the transformation of contextual information into probability maps. We validate the proposed alignment approach with two fusion type settings using the DOTA dataset. For future work, we intend to explore other fusion methods such as mid-fusion at different layers of the architecture. Additionally, we plan to evaluate the performance of the proposed approach on other datasets.

ACKNOWLEDGMENT

This work has been supported by the French National Research Agency (ANR), under the grant agreement ANR-21-ASIA-0004.

REFERENCES

- [1] W. Liu, D. Anguelov, D. Erhan, C. Szegedy, S. Reed, C.-Y. Fu, and A. C. Berg, “Ssd: Single shot multibox detector,” in *Computer Vision—ECCV 2016: 14th European Conference, Amsterdam, The Netherlands, October 11–14, 2016, Proceedings, Part I 14*. Springer, 2016, pp. 21–37.

TABLE I: Performance of the different models compared to the model without fusion (*i.e.*, Basic). Bold entries denote the best detection per target class. Green/orange/red entries show the models that are better/equal/worse compared to the Basic model.

Model	Plane	Ship	ST	BD	TC	BC	GTF	Harbor	Bridge	LV	SV	Heli.	Round.	SBF	SP	mAP	
Basic	0.76	0.47	0.63	0.62	0.77	0.40	0.39	0.65	0.26	0.59	0.34	0.30	0.46	0.50	0.14	0.48	
Basic fusion	Direct	0.78	0.47	0.62	0.66	0.77	0.54	0.50	0.62	0.28	0.60	0.33	0.24	0.39	0.53	0.13	0.50
	Indirect	0.76	0.48	0.64	0.66	0.80	0.49	0.50	0.64	0.30	0.59	0.34	0.30	0.42	0.50	0.15	0.50
Distance in Eq.1	Direct	0.79	0.47	0.66	0.60	0.80	0.44	0.62	0.64	0.41	0.58	0.34	0.46	0.53	0.48	0.18	0.53
	Indirect	0.74	0.49	0.63	0.72	0.79	0.37	0.30	0.62	0.38	0.58	0.33	0.38	0.44	0.57	0.17	0.50
Distance in Eq.2	Direct	0.78	0.48	0.62	0.67	0.78	0.54	0.53	0.68	0.35	0.61	0.34	0.31	0.49	0.55	0.21	0.53
	Indirect	0.77	0.50	0.58	0.67	0.81	0.45	0.45	0.62	0.33	0.57	0.37	0.22	0.50	0.54	0.16	0.50

TABLE II: Performance of the fusion model with one class at a time. Bold entries denote the best detection per target class. Green/orange/red entries show the classes that are better/equal/worse compared to the Basic model reported in Table I.

Model \ Class	Plane	Ship	ST	BD	TC	BC	GTF	Harbor	Bridge	LV	SV	Heli.	Round.	SBF	SP	mAP
Plane	0.75	0.47	0.61	0.67	0.78	0.52	0.51	0.62	0.27	0.61	0.35	0.26	0.44	0.47	0.15	0.50
Ship	0.75	0.49	0.62	0.62	0.79	0.43	0.42	0.62	0.24	0.57	0.33	0.33	0.47	0.51	0.19	0.49
Storage tank (ST)	0.78	0.48	0.62	0.64	0.79	0.50	0.47	0.63	0.36	0.60	0.34	0.35	0.48	0.53	0.19	0.52
Baseball diamond (BD)	0.77	0.49	0.62	0.60	0.81	0.40	0.48	0.65	0.29	0.60	0.33	0.31	0.44	0.43	0.19	0.49
Tennis court (TC)	0.78	0.48	0.61	0.64	0.81	0.42	0.44	0.65	0.29	0.60	0.34	0.33	0.39	0.43	0.15	0.49
Basketball court (BC)	0.78	0.47	0.64	0.66	0.77	0.50	0.48	0.66	0.31	0.59	0.34	0.39	0.44	0.57	0.18	0.52
Ground track field (GTF)	0.79	0.48	0.63	0.53	0.75	0.47	0.50	0.60	0.35	0.60	0.33	0.34	0.44	0.45	0.15	0.49
Harbor	0.78	0.48	0.63	0.57	0.79	0.46	0.32	0.64	0.28	0.59	0.35	0.35	0.44	0.40	0.19	0.49
Bridge	0.77	0.48	0.65	0.58	0.80	0.50	0.43	0.65	0.34	0.59	0.34	0.33	0.41	0.47	0.20	0.50
Large vehicle (LV)	0.77	0.47	0.65	0.65	0.79	0.43	0.37	0.63	0.35	0.59	0.35	0.34	0.42	0.53	0.16	0.50
Small vehicle (SV)	0.78	0.48	0.64	0.72	0.79	0.48	0.40	0.63	0.30	0.62	0.32	0.34	0.54	0.51	0.17	0.51
Helicopter	0.78	0.49	0.60	0.65	0.79	0.46	0.43	0.65	0.31	0.60	0.34	0.36	0.35	0.48	0.18	0.50
Roundabout	0.72	0.48	0.60	0.58	0.79	0.46	0.47	0.61	0.29	0.61	0.34	0.29	0.57	0.45	0.15	0.50
Soccer ball field (SBF)	0.78	0.49	0.63	0.62	0.79	0.42	0.52	0.61	0.34	0.61	0.34	0.37	0.45	0.52	0.19	0.51
Swimming pool (SP)	0.76	0.47	0.64	0.57	0.81	0.40	0.47	0.65	0.30	0.61	0.35	0.38	0.45	0.50	0.23	0.51

- J. Redmon, S. Divvala, R. Girshick, and A. Farhadi, "You only look once: Unified, real-time object detection," in *Proceedings of the IEEE conference on computer vision and pattern recognition*, 2016, pp. 779–788.
- A. Kirillov, E. Mintun, N. Ravi, H. Mao, C. Rolland, L. Gustafson, T. Xiao, S. Whitehead, A. C. Berg, W.-Y. Lo *et al.*, "Segment anything," *arXiv preprint arXiv:2304.02643*, 2023.
- J. Zhang, C. Xie, X. Xu, Z. Shi, and B. Pan, "A contextual bidirectional enhancement method for remote sensing image object detection," *IEEE Journal of Selected Topics in Applied Earth Observations and Remote Sensing*, vol. 13, pp. 4518–4531, 2020.
- C. Chen, W. Gong, Y. Chen, and W. Li, "Object detection in remote sensing images based on a scene-contextual feature pyramid network," *Remote Sensing*, vol. 11, no. 3, p. 339, 2019.
- Y. Huang, C. Du, Z. Xue, X. Chen, H. Zhao, and L. Huang, "What makes multi-modal learning better than single (provably)," *Advances in Neural Information Processing Systems*, vol. 34, pp. 10944–10956, 2021.
- G.-S. Xia, X. Bai, J. Ding, Z. Zhu, S. Belongie, J. Luo, M. Datcu, M. Pelillo, and L. Zhang, "Dota: A large-scale dataset for object detection in aerial images," in *Proceedings of the IEEE conference on computer vision and pattern recognition*, 2018, pp. 3974–3983.
- S. Ren, K. He, R. Girshick, and J. Sun, "Faster r-cnn: Towards real-time object detection with region proposal networks," *Advances in neural information processing systems*, vol. 28, 2015.
- L. Dai, H. Liu, H. Tang, Z. Wu, and P. Song, "Ao2-detr: Arbitrary-oriented object detection transformer," *IEEE Transactions on Circuits and Systems for Video Technology*, 2022.
- J. Beal, E. Kim, E. Tzeng, D. H. Park, A. Zhai, and D. Kislyuk, "Toward transformer-based object detection," *arXiv preprint arXiv:2012.09958*, 2020.
- M. Maaz, H. Rasheed, S. Khan, F. S. Khan, R. M. Anwer, and M.-H. Yang, "Class-agnostic object detection with multi-modal transformer," in *European Conference on Computer Vision*. Springer, 2022, pp. 512–531.
- N. Carion, F. Massa, G. Synnaeve, N. Usunier, A. Kirillov, and S. Zagoruyko, "End-to-end object detection with transformers," in *European conference on computer vision*. Springer, 2020, pp. 213–229.
- J. Gao, P. Li, Z. Chen, and J. Zhang, "A survey on deep learning for multimodal data fusion," *Neural Computation*, vol. 32, no. 5, pp. 829–864, 2020.
- S.-Y. Chu and M.-S. Lee, "Mt-detr: Robust end-to-end multimodal detection with confidence fusion," in *Proceedings of the IEEE/CVF Winter Conference on Applications of Computer Vision*, 2023, pp. 5252–5261.
- L. G. Brown, "A survey of image registration techniques," *ACM computing surveys (CSUR)*, vol. 24, no. 4, pp. 325–376, 1992.
- J.-G. Wang, W.-Y. Yau, A. Suwandy, and E. Sung, "Person recognition by fusing palmprint and palm vein images based on "laplacianpalm" representation," *Pattern recognition*, vol. 41, no. 5, pp. 1514–1527, 2008.
- N. Girard, G. Charpiat, and Y. Tarabalka, "Noisy supervision for correcting misaligned cadaster maps without perfect ground truth data," in *IGARSS 2019-2019 IEEE International Geoscience and Remote Sensing Symposium*. IEEE, 2019, pp. 10 103–10 106.
- L. Zhang, Z. Liu, X. Zhu, Z. Song, X. Yang, Z. Lei, and H. Qiao, "Weakly aligned feature fusion for multimodal object detection," *IEEE Transactions on Neural Networks and Learning Systems*, 2021.
- M. Yuan, X. Shi, N. Wang, Y. Wang, and X. Wei, "Improving rgb-infrared object detection with cascade alignment-guided transformer," *Information Fusion*, vol. 105, p. 102246, 2024.
- M. Arar, Y. Ginger, D. Danon, A. H. Bermanno, and D. Cohen-Or, "Unsupervised multi-modal image registration via geometry preserving image-to-image translation," in *Proceedings of the IEEE/CVF Conference on Computer Vision and Pattern Recognition (CVPR)*, June 2020.
- Y. Zhao, X. Huang, and Z. Zhang, "Deep lucas-kanade homography for multimodal image alignment," in *Proceedings of the IEEE/CVF Conference on Computer Vision and Pattern Recognition*, 2021, pp. 15 950–15 959.
- S. Waqas Zamir, A. Arora, A. Gupta, S. Khan, G. Sun, F. Shahbaz Khan, F. Zhu, L. Shao, G.-S. Xia, and X. Bai, "isaid: A large-scale dataset for instance segmentation in aerial images," in *Proceedings of the IEEE Conference on Computer Vision and Pattern Recognition Workshops*, 2019, pp. 28–37.